The Astrophysical Journal, 752:153 (8pp), 2012 June 20 doi:10.1088/0004-637X/752/2/153

THE *SWIFT* BAT SURVEY DETECTS TWO OPTICAL BROAD LINE, X-RAY HEAVILY OBSCURED ACTIVE GALAXIES: NVSS 193013+341047 AND IRAS 05218−1212

J. Drew Hogg[1], Lisa M. Winter[1,3], Richard F. Mushotzky[2], Christopher S. Reynolds[2], and Margaret Trippe[2]
[1] Department of Astrophysical & Planetary Sciences, University of Colorado, UCB 391, Boulder, CO 80309, USA;
james.hogg@colorado.edu, lisa.winter@colorado.edu
[2] Department of Astronomy, University of Maryland, College Park, MD 20742, USA
Received 2011 July 8; accepted 2012 April 19; published 2012 June 6

ABSTRACT

The *Swift* Burst Alert Telescope (BAT) is discovering interesting new objects while monitoring the sky in the 14–195 keV band. Here we present the X-ray properties and spectral energy distributions (SEDs) for two unusual active galactic nucleus sources. Both NVSS 193013+341047 and IRAS 05218−1212 are absorbed, Compton-thin, but heavily obscured ($N_{\rm H} \sim 10^{23}$ cm^{-2}), X-ray sources at redshifts <0.1. The SEDs reveal these galaxies to be very red, with high extinction in the optical and UV. A similar SED is seen for the extremely red objects (EROs) detected in the higher redshift universe. This suggests that these unusual BAT-detected sources are a low-redshift ($z \ll 1$) analog to EROs, which recent evidence suggests are a class of the elusive type II quasars. Studying the multi-wavelength properties of these sources may reveal the properties of their high-redshift counterparts.

Key words: galaxies: active – galaxies: Seyfert – surveys – X-rays: galaxies

Online-only material: color figures

1. INTRODUCTION

Supermassive black holes are believed to exist at the centers of most massive galaxies. While a connection between the central black hole and larger host galaxy has been observationally proven (the M–σ relation), there are still many unanswered questions as to how the central black hole affects the host galaxy's formation and evolution. Since previous studies of active galactic nuclei (AGNs) have relied heavily on optically or X-ray-selected samples, they missed a significant fraction (≈20%) of AGNs—the heavily obscured sources (Ueda et al. 2007; Winter et al. 2008, 2009a). Thus, our understanding of the AGNs and their connection to the host is missing a potentially key parameter.

Surveys of AGNs are typically dominated by two selection effects: dilution by starlight from the host galaxy and obscuration by dust and gas in the host galaxy and the AGN itself (see Hewett & Foltz 1994 and Mushotzky 2004). These factors previously kept an unbiased AGN sample from reach. However, with the capabilities of *Swift*'s Burst Alert Telescope (BAT), this has changed. The BAT surveys the sky in the hard X-ray range of 14–195 keV. In the first 22 months of the survey, BAT detected ∼250 AGNs with a median redshift of 0.03 (Tueller et al. 2010). These AGNs were selected purely by their hard X-ray flux, and thus are not affected by obscuration by gas and dust below ≈10^{24} cm^{-2}, which prevents them from being easily detected in optical or soft band X-ray surveys.

In the BAT sample there is no bias against detecting heavily obscured but still Compton thin AGNs, and thus the sample offers a unique test of the unified model of AGNs (Antonucci 1993). In the unified model, differences between broad (type 1) and narrow-line (type 2) AGNs are attributed to differences in the viewing angle to the central, obscured region (Osterbrock 1978). Therefore, there should be no differences between the X-ray and optical AGN classifications.

However, the X-ray/optical properties of two sources out of the ≈ 250 detected do not fit the most basic prediction of the unified model. Both NVSS 193013+341047 and IRAS 05218−1212 show broad optical lines indicative of a type 1–1.5 optical source, but the low resolution *Swift* XRT spectra indicated that the sources were likely highly absorbed. Further, the combined BAT and XRT X-ray spectra indicated that the sources were mildly "Compton-thick," with column densities of $N_{\rm H} > 1.4 \times 10^{24}$ cm^{-2}. The spectral energy distributions (SEDs) of these sources are extremely red, showing very heavy extinction levels in the UV and soft X-rays (<2 keV). Such SEDs have only previously been seen for the high-redshift ($z \gtrsim 1$) extremely red objects (EROs). In order to determine the X-ray properties of these sources, we obtained X-ray follow-ups with *XMM-Newton*. In this paper, we present both the X-ray and broadband properties of these two unusual sources detected in the *Swift* BAT survey.

2. X-RAY SPECTRA

2.1. Observation Details

XMM-Newton follow-ups were acquired in the 0.1–10 keV band for both NVSS 193013+341047 and IRAS 05218−1212. Basic details of the sources and the *XMM-Newton* observations are included in Table 1. The spectra were processed and extracted using the Science Analysis System (SAS) version 9.0. We followed the process for reduction outlined in the *XMM-Newton* ABC Guide.[4] First, we created calibrated photon event files for the EPIC MOS and pn cameras using the observation data files (ODFs) with the commands `emchain` and `epchain`, respectively.

The events tables were filtered using standard filters as outlined in the ABC Guide. For MOS data, good events constitute those with a pulse height in the range of 0.2–12 keV and event patterns that are characterized as 0–12 (single, double,

[3] Hubble Fellow.

[4] The ABC Guide is available online at http://heasarc.nasa.gov/docs/xmm/abc/.

Table 1
Details of the *XMM-Newton* Observations

Source	R.A.	Decl.	z	Obs. ID	Date	Exp. Time[a]	⟨Count Rate⟩[a]
NVSS 193013+341047	19:30:13.86	+34:10:50.04	0.0629	0602840101	2009 May 16	12.91	0.29
IRAS 05218−1212	05:24:06.80	−12:10:10.87	0.0490	0551950401	2008 Aug 24	11.27	0.17

Note. [a] The exposure time (in units of ks) and count rate (in units of counts s^{-1}) are recorded for the pn spectra in the 0.1–10 keV band.

triple, and quadruple pixel events). For the pn camera, only patterns of 0–4 (single and double pixel events) are kept, with the energy range for the pulse height set between 0.2 and 15 keV. Bad pixels and events too close to the edges of the CCD chips were rejected using the most stringent selection expression, FLAG == 0, for both data sets. Based on an inspection of the light curve, we found no evidence of flaring in either observation. Therefore, we did not apply any temporal filtering.

The spectra of the sources were extracted using the SAS task `evselect`. The spectra were extracted in a circular aperture centered on the source. Additionally, background spectra were extracted with a circular aperture of the same size, in a region nearby the source on the same CCD chip, but free of additional X-ray sources. Response files were generated using the SAS tasks `rmfgen` and `arfgen`. The spectra were then binned by 20 counts per bin using `grppha`.

In addition to the *XMM-Newton* spectra, we also obtained *Swift* BAT spectra. The spectra are time-averaged over 22 months and are fully described in Tueller et al. (2010).[5] The BAT spectra cover the 14–195 keV band and consist of eight energy bins with edges of 14, 20, 24, 35, 50, 75, 100, and 150 keV.

2.2. XMM-Newton Light-curve Analysis

In order to search for variability in each of the sources, we created background subtracted light curves for pn in a soft (0.3–3 keV), medium (3–7 keV), and hard (7–10 keV) band, using a bin size of 128 s. The same source and background regions were used as those to extract the spectra. For NVSS 193013+341047 the average background subtracted count rate in each band was 1.88×10^{-2} counts s^{-1} (soft), 4.79×10^{-2} counts s^{-1} (medium), and 1.69×10^{-2} counts s^{-1} (hard). For IRAS 05218−1212, the average count rate was 5.15×10^{-2} counts s^{-1} (soft), 4.67×10^{-2} counts s^{-1} (medium), and 9.98×10^{-3} counts s^{-1} (hard).

As a simple search for variability, we computed $\chi^2 = \sum(C_i^2 - \mu^2)/\sigma^2$ for each light curve, where C_i is the background subtracted count rate in each bin, μ is the average count rate, and σ is the error. For NVSS 193013+341047, the reduced χ^2 values are 0.85 (soft), 0.69 (medium), and 1.13 (hard), where the light curves had 113 dof. For IRAS 05218−1212, the reduced χ^2 values are 0.77 (soft), 1.09 (medium), and 1.09 (hard), where the light curves had 101 dof. The amount of variability is low in all of the light curves. However, the medium band, which encompasses the Fe Kα emission region, corresponds to the greatest variability in NVSS 193013+341047 and the soft band corresponds to the greatest variability in IRAS 05218−1212. The band with the greatest short-term variability for each source also corresponds to the band with the highest count rate. While we do not present the results of the MOS light-curve analysis, we find that the MOS results are in agreement with the pn.

[5] *Swift* BAT spectra for the 22 month sample are publicly available at http://heasarc.nasa.gov/docs/swift/results/bs22mon/.

2.3. Spectral Fitting

Spectral fitting was done using XSPEC v12.4 (Arnaud 1996). The spectral fit of NVSS 193013+341047 is presented in Figure 1 and the spectral fit of IRAS 05218-1212 is presented in Figure 2. For each of the sources, we simultaneously fit the *XMM-Newton* EPIC (pn + MOS) spectra with the *Swift* BAT spectra, covering a wavelength range from 0.3–195 keV. As an initial fit to the spectra, we used a power-law model absorbed by the Galactic column density in the line of sight, in XSPEC `tbabs*powerlaw`, to each source ($N_{\rm H} = 1.73 \times 10^{21}$ cm^{-2} for NVSS 193013+341047 and $N_{\rm H} = 9.83 \times 10^{20}$ cm^{-2} for IRAS 05218−1212, as obtained from Dickey & Lockman 1990). We added a flux constant to the model to account for differences in the flux between the pn spectrum and each of the MOS and BAT spectra. This simple model was not a good fit to either spectrum, with $\chi^2/{\rm dof} = 943/330$ (reduced $\chi^2 = 2.9$) for NVSS 193013+341047 and 1184/307 (reduced $\chi^2 = 3.9$) for IRAS 05218−1212.

In Winter et al. (2008, 2009a), we describe our choice of a partially covering absorption model (`pcfabs` in XSPEC) to fit more complex spectra in the *Swift* AGN catalog. This model, $M(E) = f_{\rm cover} \times \exp^{-N_{\rm H}\sigma(E)} + (1 - f_{\rm cover})$, assumes that the intrinsic absorbing column density only partially covers the AGN emission and that some portion of the direct emission is not blocked by the obscuring region. Adding this model to each of our source spectra, we find a large statistical improvement in the fit ($\Delta\chi^2$ is 127 for NVSS 193013+341047 and 586 for IRAS 05218−1212).

In addition to the partially covering absorption model, we added a reflection model, `pexrav` (Magdziarz & Zdziarski 1995), to account for X-ray emission reflected into the line of sight. The parameters of this model include the power-law index and normalization, which we fixed to the values of the direct emission, the reflection factor ($R = \Omega/2\pi$, where Ω is the solid angle over which the material is reflected), the source redshift, cutoff energy, and the inclination angle (which we fix at the default of $\cos\theta = 0.45$). Negative values for the reflection factor indicate a pure reflection spectrum. Therefore, we allowed this parameter to vary within the range of 0 to −5. The addition of the reflection model was a significant improvement to the fits for both spectra, with $\Delta\chi^2$ of 24 for NVSS 193013+341047 and 31 for IRAS 05218−1212. However, we could not constrain the cutoff energy (instead we fixed this to 100 keV) or the reflection parameters.

The final component added to our spectral model was a Gaussian line (`zgauss`) to fit the Fe Kα emission. A line was statistically significant in both sources, with $\Delta\chi^2$ of 17 for NVSS 193013+341047 and 21 for IRAS 05218−1212. In addition to the Fe Kα emission at 6.41 keV, the spectrum of IRAS 05218−1212 is more complex. In Figure 3, we show the ratio of the data/model in the 5–8 keV band for this source with the best-fit model, excluding the Gaussian added to fit Fe Kα. The most significant line is clearly the narrow 6.41 keV emission. Also present is a narrow emission line at 6.0 keV.

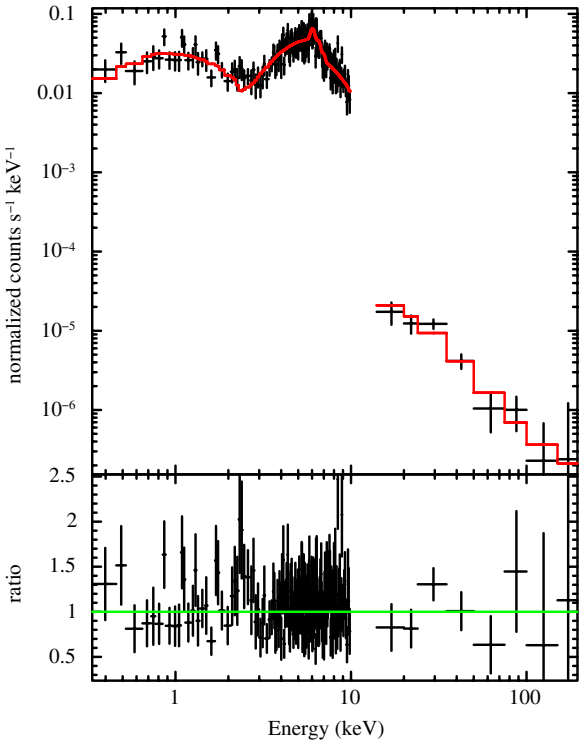

Figure 1. *XMM-Newton* pn and *Swift* BAT spectra are plotted for NVSS 193013+341047, along with the best fit model, as well as the ratio of the data/model in the bottom plot. The spectrum is complex and required a partial covering absorber model.

(A color version of this figure is available in the online journal.)

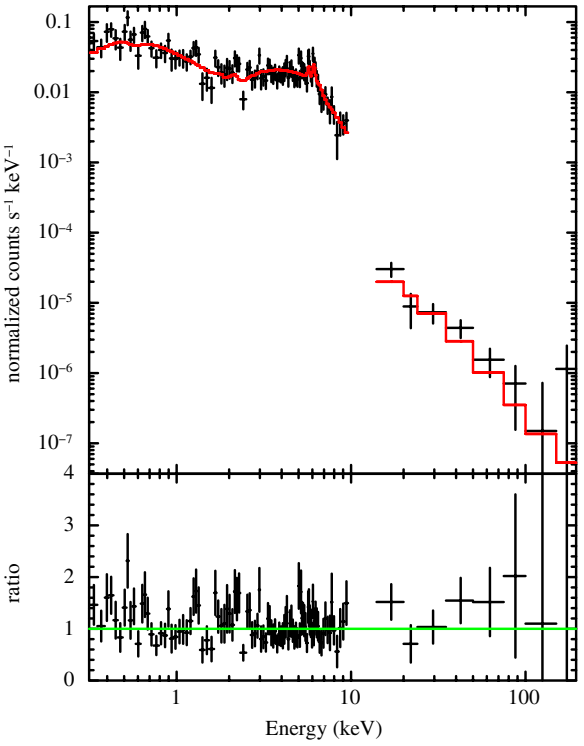

Figure 2. *XMM-Newton* pn and *Swift* BAT spectra are plotted for IRAS 05218−1212, along with the best fit model, as well as the ratio of the data/model in the bottom plot. The spectrum is complex and required a partial covering absorber model.

(A color version of this figure is available in the online journal.)

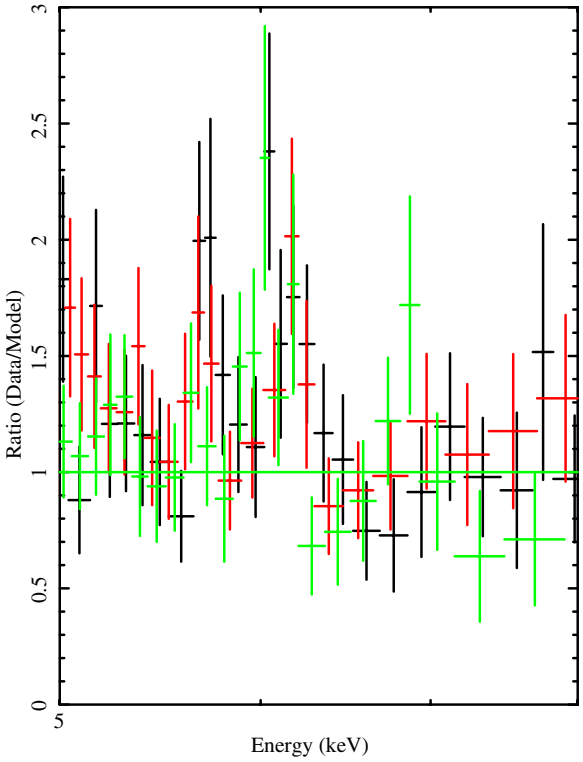

Figure 3. Ratio of the data/model for a partially covering power-law model without accounting for the Fe Kα emission is shown in the 5–8 keV band. The pn (black), MOS1 (red), and MOS2 (green) data points are shown. In addition to the narrow Fe Kα line at 6.41 keV, a second line is significant in each of the detectors ($\Delta\chi^2 = 9$) at 6.0 keV.

(A color version of this figure is available in the online journal.)

Table 2
Joint *XMM-Newton* and BAT Spectral Fits

Parameter	NVSS 193013+341047	IRAS 05218−1212
$N_{\rm H}$[a]	$24.5^{+3.7}_{-4.8}$	$10.9^{+0.81}_{-0.77}$
$f^{\rm a}_{\rm cover}$	$0.93^{+0.02}_{-0.03}$	$0.93^{+0.01}_{-0.01}$
$\Gamma^{\rm b}$	$1.42^{+0.10}_{-0.13}$	$2.11^{+0.09}_{-0.10}$
$A_\Gamma{}^{\rm b}$	9.85×10^{-4}	1.74×10^{-3}
$R^{\rm b}$	(-5)	(-5)
$E^{\rm c}_{\rm FeK\alpha}$	$6.38^{+0.07}_{-0.08}$	$6.41^{+0.06}_{-0.06}$
$\sigma^{\rm c}$	$0.14^{+0.13}_{-0.08}$	$0.07^{+0.06}_{-0.07}$
EW[c]	149^{+79}_{-65}	172^{+137}_{-63}
χ^2/dof	292/323	302/300

Notes.
[a] Parameters of the `pcfabs` model, including hydrogen column density measured in units of 10^{22} atoms cm^{-2} and the covering fraction of the absorber. [b] Spectral index computed with the reflection model `pexrav` assuming total reflection and a fixed energy cutoff at 150 keV. The reflection parameter is not well constrained. The quoted normalization on the power-law component is in units of photons keV^{-1} cm^{-2} s^{-1} at 1 keV. [c] Equivalent width and normalization (with errors or as an upper limit) on a fixed Gaussian Fe K line at 6.41 keV in units of eV and $10^{-5}\times$ total photons cm^{-2} s^{-1}, respectively.

Full details of our best-fit spectral parameters are presented in Table 2. A similar analysis is found in Trippe et al. (2011) for IRAS 05218−1212, which uncovers similar best-fit values as our analysis. To summarize our results from the spectral fits, we find that the spectra of both sources are heavily absorbed with $N_{\rm H} \geqslant 10^{23}$ cm^{-2}, but Compton thin. The absorption is

partially covering, covering approximately 93% of the emission in both sources. The measured power-law indices of both sources deviate from the average value of 1.75 found for the *Swift* BAT sample (Winter et al. 2009a), with Γ being flat for NVSS 193013+341047 (1.42) and steep for IRAS 05218−1212 (2.11). Reflection is statistically significant in both sets of spectra, but not well constrained. Additionally, an Fe Kα emission line is present in both spectra with an equivalent width of ≈150 eV. The width of this line is slightly broad, with $\sigma = 0.14$ keV, for NVSS 193013+341047.

3. COMPARISON WITH OTHER BANDS

On the basis of the X-ray spectra alone, these two AGNs clearly have complex X-ray spectra. With higher signal-to-noise X-ray spectra, Winter et al. (2009a) found that more than 50% of the 153 9-month BAT AGN have complex spectra well fit by a partial covering model. Among these, nearly all were absorbed sources ($N_{\rm H} > 10^{22}$ cm^{-2}). While the initial *Swift* XRT + BAT fits suggested that these sources were Compton-thick candidates, our *XMM-Newton* observations reveal that NVSS 193013+341047 and IRAS 05218−1212 are Compton thin. However, the high column densities above 10^{23} cm^{-2} and covering fractions >90% show that these are likely hidden/buried AGNs. This is a new class of objects, comprising 24% of the *Swift* AGNs, uncovered in high energy surveys, whose AGN nature is hidden in the optical/soft X-rays due to obscuring gas and dust (Ueda et al. 2007; Winter et al. 2009a, 2009b). The most interesting properties of these sources, however, are evident when comparing the X-ray properties with other wavelengths. These include a mismatch between the optical and X-ray classifications and unusually red SEDs.

3.1. Optical

Both the optical spectra of NVSS 193013+341047 and IRAS 05218−1212 show clear broad lines, leading to an optical classification of Sy 1–1.8, typically associated with an unabsorbed AGN. For NVSS 193013+341047, it is unlikely that the X-ray/optical mismatch is due to variability since the broad lines were evident in two spectra taken over three months apart (Landi et al. 2007 and Winter et al. 2010a). Further, *Swift* XRT spectra, indicating the X-ray spectrum to be absorbed, were also taken within a few months of the optical. For IRAS 05218−1212, an EXOSAT spectrum, taken within 2 years of the optical spectrum of Morris & Ward (1989), showed the 2–10 keV X-ray band to be a factor of 10 times underluminous compared to other *IRAS*-selected AGNs (Ward et al. 1988), indicating that the source was likely heavily absorbed at this time. Additionally, an optical spectrum from 2009 April 22, presented in Trippe et al. (2011), also confirms the optical broad emission line spectrum. Thus, the mismatch between X-ray and optical spectra is unlikely due to variability in the sources. Further, the optical polarization fraction of IRAS 05218−1212 was reported as less than 1% (Brindle et al. 1990), showing that the optical light is not mostly scattered around the X-ray obscuring region.

In the *XMM* large-scale structure survey, 7 out of 61 (11%) optical broad-line sources exhibited X-ray absorbed spectra (Garcet et al. 2007). It is interesting to note that all of these sources are more luminous (in $L_{2-10\,\rm keV}$ by ≈100) and at much higher redshift ($\langle z \rangle = 1.93$) than our target sources. Similar sources have been found by Perola et al. (2004) and Eckart et al. (2006), comprising 5%–15% of their X-ray samples. Thus, our targets may be the first low-redshift AGN discovered from this class of object, which includes a significant fraction of high-redshift AGNs. As the low-redshift analogs of this class, we will be able to study the sources and hosts, in particular, in much greater detail due to their much closer distance.

3.2. Infrared

Not only are the X-ray and optical spectra of our targets puzzling, but both sources are very red, with $J - K = 2.43$ (NVSS 193013+341047) and 1.74 (IRAS 05218−1212). These values are high compared to the nine month BAT AGN sample, taken from NED. In Figure 4, we plot the Two Micron All Sky Survey (2MASS) $J - K$ values for the nine month sample versus both X-ray absorbing column and the 14–195 keV luminosity, obtained from Winter et al. (2009a). These plots show a few interesting results. First, Sy1s (triangles) are redder than Sy2s (circles), with the average $J - K$ of 1.32 for the 31 Sy 1–1.5 s, 1.13 for the 26 Sy 1.5–1.9 s, and 1.07 for the 30 Sy2s. The high $J - K$ values of NVSS 193013+341047 and IRAS 05218−1212 align them more closely with the Sy1s. This also causes our sources, along with 3C 105, to inhabit a strange place in the plot of $J - K$ versus $N_{\rm H}$, being higher column density sources with higher $J - K$ values. 3C 105, however, is unlike our sources in that it is a narrow-line radio galaxy which does not exhibit broad optical lines.

Another interesting result we find is that the sources with the highest $J - K$ values are also the most luminous of the BAT sample. In addition to NVSS 193013+341047 and IRAS 05218−1212, 3C 105, 3C 111.0, 3C 273, and EXO 055620−3820 are the most luminous sources with the highest $J - K$. Among these, only 3C 105 has a high column density. The host galaxies of both 3C 105 and 3C 111.0 are identified as ellipticals from *Hubble Space Telescope* observations with NICMOS (Madrid et al. 2006). 3C 273 is a blazar, while EXO 055620−3820 is an Sy1 with a complex X-ray spectrum best-fit by an ionized partial covering model (Turner et al. 1996). The host types are unknown for both of these sources. Both NVSS 193013+341047 and IRAS 05218−1212 are unusual, even among the most luminous and highest $J - K$ sources in the sample, in having a mismatch between the X-ray and optical types. While the X-ray spectra are similar to 3C 105, this source exhibits no optical broad lines.

3.3. Broadband SEDs

In Figure 5, we show the observed broadband SEDs for both NVSS 193013+341047 and IRAS 05218−1212. The radio/IR data includes publicly available flux densities from NVSS, *IRAS*, and 2MASS (obtained through the NASA/IPAC Extragalactic Database). In addition to this, we include our own measurements from *Swift* BAT and *XMM-Newton*—including both the observed X-ray measurements based on our best-fit model and Optical/UV measurements from the Optical Monitor (OM) and the *Swift* UV/optical telescope (UVOT).

Data from the OM were available in the *U* and *UVW1* filters for IRAS 02218−1212 and in the *UVW1* filter for NVSS 193013+341047. We processed the OM data with the SAS script `omichain`. The flux and magnitudes were extracted with the interactive SAS package `omsource`, using a 6″ circular aperture centered on the source and a circular background region, free of sources. We also include *Swift* UVOT observations for our target sources, which were obtained using the same region files as for the OM data, and extracted with

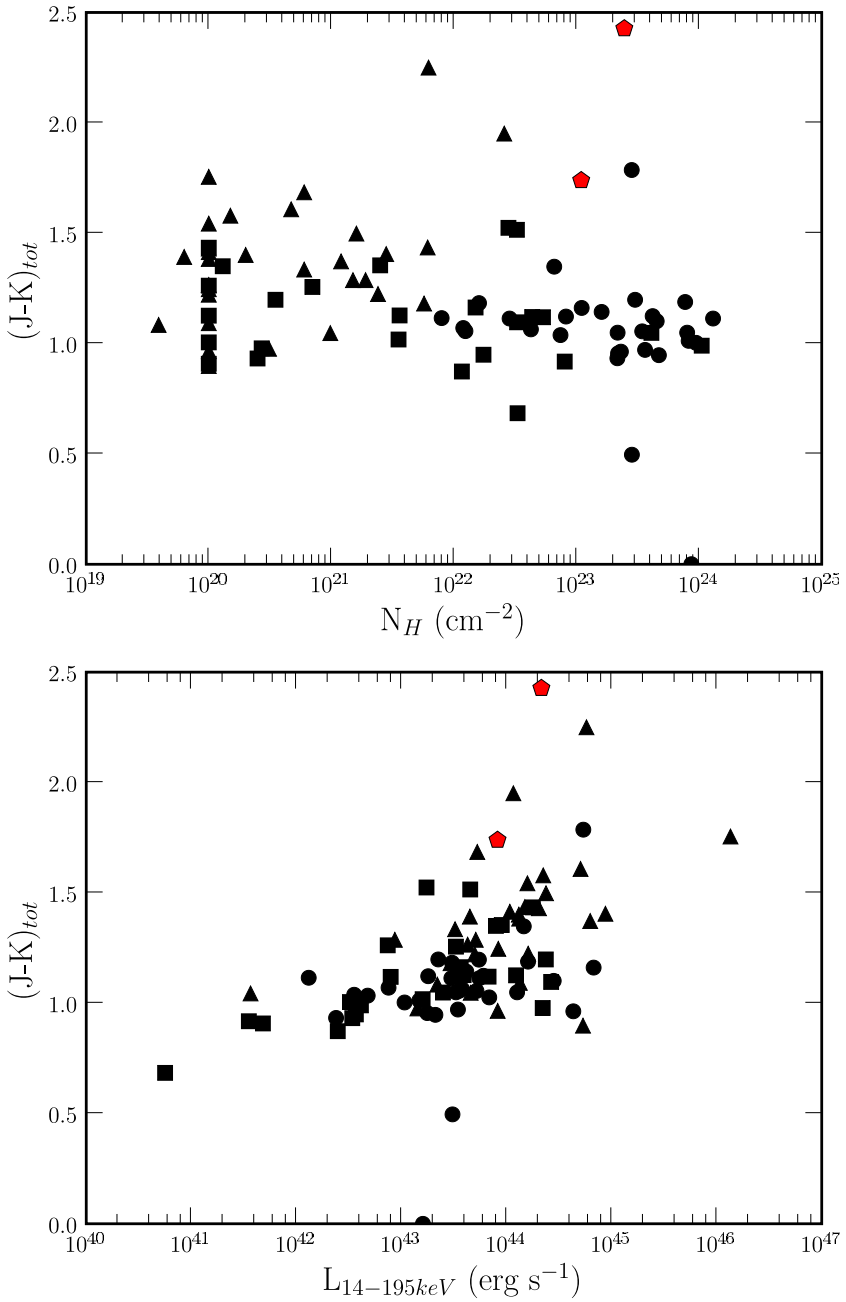

Figure 4. Plot of reddening vs. the X-ray-measured column density ($N_{\rm H}$) and the 14–195 keV luminosity from BAT. The reddening ($J-K$) is constructed from the 2MASS values, publicly available in NED. NVSS 193013+341047 and IRAS 05218−1212 (pentagons) are among the reddest sources, along with 3C 111.0, EXO 055620−3820, 3C 105, and 3C 273. Seyfert 1–1.5 sources (triangles), Seyfert 1.5–2 (squares), and Seyfert 2 s (circles) are all indicated.

(A color version of this figure is available in the online journal.)

the *Swift* tool `uvotsource`. Processed *Swift* UVOT observations were available in the *V*, *B*, *U*, *UVW1*, *UVM2*, and *UVW2* bands for NVSS 193013+341047 (with *Swift* observations 00035274002 and 00035274003) and the *V*, *UVM2*, and *UVW2* bands for IRAS 02218−1212 (*Swift* observations 00037085001, 00037085002, 00037085003, and 00037085004). Our broadband SEDs also include the X-ray flux densities measured in the 0.5–2 keV, 2–10 keV, and 14–195 keV bands, based on our joint XMM + BAT spectral fits. The measurements are included in Table 3.

The SEDs for both sources, particularly for NVSS 193013+341047, show the sources to be very bright in the IR with sharp declines in flux into the UV and soft X-rays. While bright IR emission could be the result of reprocessing of the AGN emission in dust, which obscures the optical/soft X-rays, it is still unclear as to why there are optical broad lines. We are unaware of any other low-redshift AGN of type 1 or 2 with similar SEDs. While other red AGNs ($J-K>2$) have been selected through 2MASS, X-ray follow-ups have not shown the same mismatch between X-ray and optical spectra (Wilkes et al. 2005).

4. DISCUSSION

4.1. Optical and X-Ray Reddening

Multi-wavelength observations of active galaxies previously revealed differences in the reddening measured between X-ray and optical spectroscopy. Assuming a standard Milky

Table 3
Multi-wavelength Flux Measurements

SED Data		NVSS 193013+341047	IRAS 05218−1212
Measurement	ν (Hz)	F_ν (mJy)	F_ν (Jy)
NVSS	1.4×10^9	4.4 ± 0.6	9.2 ± 1.1
IRAS 100μ	3×10^{12}	···	1020
IRAS 60μ	5×10^{12}	···	456.3 ± 50
IRAS 25μ	1.2×10^{13}	···	280
IRAS 12μ	2.5×10^{13}	···	100
2MASS K_s	1.388571×10^{14}	12.6	16.5
2MASS H	1.803805×10^{14}	6.05	11.3
2MASS J	2.427469×10^{14}	3.2	7.95
UVOT B	6.662055×10^{14}	0.277 ± 0.049	···
UVOT B	6.662055×10^{14}	0.26 ± 0.01	···
OM U	$8.30781414 \times 10^{14}$	···	2.41 ± 0.10
UVOT V	8.446×10^{14}	0.78 ± 0.09	6.15 ± 0.10
UVOT U	$8.81742524 \times 10^{14}$	0.13 ± 0.02	···
UVOT U	$8.81742524 \times 10^{14}$	0.196 ± 0.019	
OM *UVW1*	$9.82092118 \times 10^{14}$	0.05 ± 0.01	2.10 ± 0.01
UVOT *UVM2*	1.297803×10^{15}	0.027 ± 0.006	1.49 ± 0.01
UVOT *UVM2*	1.297803×10^{15}	0.024 ± 0.007	1.64 ± 0.02
UVOT *UVW2*	1.414115×10^{15}	0.030 ± 0.005	1.41 ± 0.02
UVOT *UVW2*	1.414115×10^{15}	···	1.54 ± 0.02
PN soft	$1.25643545 \times 10^{17}$	0.00010	0.00036
PN hard	$1.89640880 \times 10^{18}$	0.00015	0.00027
BAT	$6.01787337 \times 10^{18}$	0.00013	0.00029

Notes. The NVSS, *IRAS*, and 2MASS flux densities were obtained using the NASA/IPAC Extragalactic Database. *Swift* UVOT and *XMM-Newton* OM observations were analyzed as explained in the text. The X-ray measurements, obtained from the best-fit X-ray models, correspond to the 0.5–2 keV soft band, 2–10 keV hard band, and the 14–195 keV BAT band fluxes.

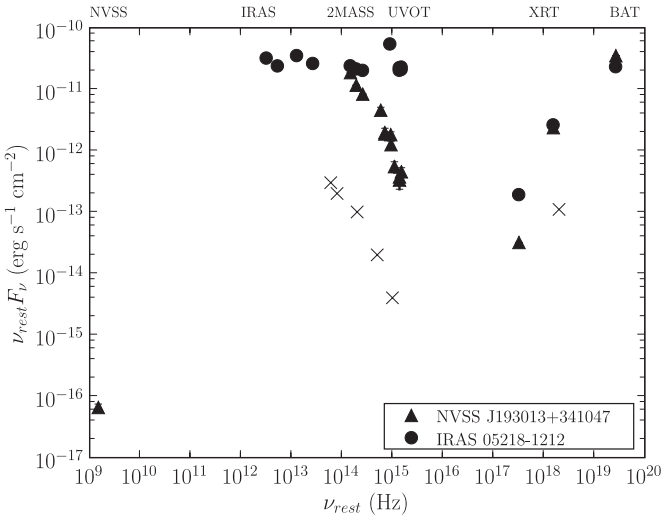

Figure 5. We constructed the observed spectral energy distributions (SEDs) for our targets using available radio/*IRAS*/2MASS measurements as well as our own measurements from the *Swift* and *XMM-Newton* observatories (including optical/UV from UVOT and *XMM* OM, 0.5–10 keV X-rays with XRT/*XMM* pn, and 14–195 keV very hard X-rays with BAT). Both sources show a steep decline in flux from infrared into ultraviolet and soft X-rays, not typical of the other BAT AGNs. However, the sharp drop in flux from the IR to UV/soft X-rays is similar to the SED of ERO source XBS J0216−0435 (Severgnini et al. 2006), plotted with the cross symbols.

Way extinction curve and dust-to-gas ratio, derived X-ray column densities can be up to ten to one hundred times that of estimates based on optical emission lines (e.g., Mushotzky 1982; Maccacaro et al. 1982; Maiolino et al. 2001b). In the *Swift* sample, optical estimates of the reddening from the ratio of narrow Hα/Hβ emission lines show this same trend with the X-ray-derived hydrogen columns 10–100 times larger than the optically derived column densities (Winter et al. 2010b). For NVSS 193013+341047 in particular, our estimate of the reddening from the ratio of narrow Hα/Hβ is $E(B-V) = 0.16$ (Winter et al. 2010a), corresponding to an optically derived column density of 8.5×10^{20} cm^{-2} (based on the conversion from Maiolino et al. 2001b). Therefore, for this source the X-ray-derived column is nearly 300 times larger than the optically derived column, on the extreme end of what is typically found for differences in the optical/X-ray-derived reddening values.

There are a number of ideas in the literature about how to account for differences in the X-ray/optical obscuration. One possible explanation for mismatches in the optical/X-ray reddening is that the dust-to-gas ratio for AGNs is lower than in the interstellar medium in our own Galaxy. Maiolino et al. (2001a) suggest that large dust grains in the region around the AGN are responsible for the differences between the estimates of the optical and X-ray reddening. Among the evidence for unusual dust properties, Maiolino et al. (2001b) show that active galaxies have faint to no detection of the silicate features at 9.7 μm and the 2175 Å carbon feature, both of which indicate the presence of small dust grains. Several other possibilities to explain the optical/X-ray mismatch that are discussed in these papers include higher metallicities in active galaxies, the hard X-rays being absorbed by the optical broad emission line producing clouds (which are expected to have $N_{\rm H} \sim 10^{23}$ cm^{-2}), and scattering of the broad-line emission through a region of lower column density than what obscures the X-ray emission. Alternatively, Shi et al. (2006) propose an accretion disk geometry that can explain the X-ray

obscuration and 9.7 μm silicate feature. Yet another explanation for differences in reddening is that the X-ray absorption is related to an AGN-driven wind. We describe this possibility in the following sub-section.

4.2. Ionized Emitters

Mismatches in classification between the X-ray absorbed and broad-line optical spectra are sometimes explained by the presence of a high column of ionized gas. Such a model has been adopted to account for active galaxies at both low and high redshift. For instance, the optical and UV spectra of the low-z AGN NGC 4151 reveal broad emission lines while the X-ray grating observations show that the soft X-rays are heavily obscured and dominated by strong ionized emission (e.g., Kraemer et al. 2005). NGC 4151 is classified similarly as an Sy 1.5, with a strongly detected multiple-component ionized outflowing wind in the UV/X-rays (Kraemer et al. 2005, 2006). NGC 4151 is also detected in the *Swift* catalog; however, both the amount of reddening (from $J-K$) and the column density of gas are much lower than the two new sources we present in this current paper, showing that it is not a useful analog for heavily reddened NVSS 193013+341047 and IRAS 05218−1212.

Perhaps a more relevant example of a source with a mismatch between optical and X-ray spectra is the broad-line radio galaxy 3C 445, which is at a similar redshift to our sources with $z = 0.057$. Broad emission lines are observed in this source (FWHM $\sim$ 6400 km s^{-1}) along with a highly reddened continuum ($E_{B-V} = 1$ mag; Crenshaw et al. 1988). *Suzaku* and *Chandra* observations show that 3C 445 is heavily absorbed with a column density of $\sim 10^{23}$ cm^{-2} and that the soft spectrum, like that of NGC 4151, is dominated by emission lines (Braito et al. 2011). Braito et al. (2011) conclude that the photoionized emitting gas is likely associated with the broad-line region (BLR) gas, which we are able to view because the high column density absorber is not completely blocking the BLR. This is possible if the obscuring region is not a uniform torus but instead clumpy or wind-like in structure (e.g., Risaliti et al. 2002 and Elitzur 2008).

In both NVSS 193013+341047 and IRAS 05218−1212 the residuals in the soft X-rays of our spectra suggest that emission lines may be present, but our observations do not have the resolution to confirm them. If higher resolution X-ray observations indicate both the high column density neutral obscuration and a strong emission component, then the same clumpy torus/wind models used to explain NGC 4151 and 3C 445 also explain the mismatch in classifications for our unusual sources. To confirm strong emission, potentially associated with an outflow, we will propose for grating observations of these sources with *XMM-Newton*/*Chandra*.

Recently, active galaxy/quasar driven outflows were also invoked to explain highly absorbed QSOs detected with *ROSAT*/submillimeter surveys (Page et al. 2011). In this case, the $z \sim 2$ QSOs with rest-frame broad UV emission lines and heavily absorbed X-rays have X-ray spectra that can be modeled with ionized absorption. Alexander et al. (2005) suggest that these sources may be in a transition between the absorbed and unabsorbed phases. As Page et al. (2011) show, this stage may be marked by strong AGN-driven winds. If this is the case, then the intermediate Seyfert 1 types, like the newly detected *Swift* sources we discuss in this paper, are likely in a similar transitional stage. This is supported by the fact that many of the well-known Seyferts with strong outflow detections are Sy 1.5 s (e.g., NGC 3516, NGC 3783, and NGC 4151).

4.3. Low-redshift EROs?

While there are no known low-redshift AGNs with similar SEDs to NVSS 193013+341047 and IRAS 05218−1212, the high-redshift universe does provide a useful analog. Namely, we find that the SEDs of our sources, particularly NVSS 193013+341047, match that of XBS J0216−0435 ($z \approx 2$). This source is identified as a type 2 quasar hosted in an ERO, whose SED is presented in Severgnini et al. (2006). In Figure 5, we include the SED of this source with a cross symbol. As pointed out and illustrated in Figure 6 of Severgnini et al. (2006), the SED is unlike those of radio-quiet or radio-loud AGNs.

EROs are identified as red sources with $R - K \gtrsim 5$ (Elston et al. 1988) or $I - K \gtrsim 4$. Joint IR/X-ray studies of EROs have found that most AGNs in this category are heavily obscured ($N_{\rm H} > 10^{22}$ cm^{-2}; Alexander et al. 2002). Based on the 2MASS (J, H, K) colors, we estimate $R-K$ of 4.8 (NVSS 193013+341047) and 3.5 (IRAS 05218−1212). This places them below the formal definition of an ERO. However, with a similar SED, very red colors, and X-ray absorbed spectra, our sources may be the low-redshift equivalent. Particularly, the result showing $J-K$ values to increase with increasing luminosity (Figure 4), supports this claim, as our sources are a factor of 10–100 less luminous in the 2–10 keV X-ray band. If these sources are low-redshift EROs, then multi-wavelength studies of their properties will help to answer many of the questions surrounding these high-redshift sources.

Previous X-ray observations of EROs suggest that they are absorbed sources with $N_{\rm H} > 10^{22}$ cm^{-2}, representing a class of type II quasars (Mignoli et al. 2004; Brusa et al. 2005). These type II quasars all tend to be hosted within elliptical galaxies. While we can not be sure of the morphology of NVSS 193013+341047 and IRAS 05218−1212, no spiral arms are distinguished in the available Digital Sky Survey images. The morphologies of *Swift*-detected AGNs with similar $J-K$ colors all tend to be in ellipticals, so it is possible that our unusual sources are also hosted in ellipticals. If so, our highly reddened active galaxies are two of only a handful of *Swift*-detected AGNs with elliptical hosts, as the majority of the very hard X-ray-detected galaxies are associated with spirals (Koss et al. 2011).

5. SUMMARY

In this paper, we present two very unusual AGNs discovered by the *Swift* BAT all-sky survey. In the X-ray band, these sources are clearly heavily absorbed ($N_{\rm H} = 1$–2×10^{23} cm^{-2}), with little X-ray flux below 2 keV. Both of these sources exhibit broad lines in their optical spectra, seemingly at odds with the heavily absorbed X-ray spectra. Further, the SEDs, revealed through publicly available NVSS, *IRAS*, 2MASS, and *Swift* data, are very red. As such, these sources appear to be the low-redshift analogs of AGNs hosted in EROs. It is still unclear, however, how the multi-wavelength properties fit together, particularly the mismatch between X-ray and optical classification, but one possible explanation is that the heavy obscuring column density is only partially obscuring the BLR, as well as an associated X-ray emitting region associated with an outflow. High signal-to-noise grating observations are required to confirm outflowing ionized gas in the spectra of these sources.

Another possible explanation for the mismatch in classifications is that the dust properties in the host galaxies of NVSS 193013+341047 and IRAS 05218−1212 are different. Infrared spectroscopy could help to uncover the dust

properties in these sources. What we can discern, on a larger scale, is that the host galaxy types of these unusual sources may be different from the majority of the BAT-selected sample. From the 2MASS-derived absolute magnitudes of $J = -22.8$ and -23.78, we find that the host galaxies are of typical luminosity (L_*). Unfortunately, the available images from UVOT and the Digital Sky Survey, are not of sufficient quality to resolve structure, determine whether the sources are actively undergoing star formation, or discern dust lanes. Since spiral arms are not indicated and two of the BAT AGN with high 14–195 keV luminosities and similar $J - K$ values are hosted in ellipticals, it is possible that the hosts of these sources are also ellipticals. If this is the case, the sources are particularly interesting, being among only $\approx 5/100$ BAT AGNs known to be hosted in an elliptical.

Finally, and possibly most importantly, we showed that the 2MASS-derived $J - K$ values for the BAT AGN appear to be connected to both the amount of X-ray obscuration and the 14–195 keV luminosity. We showed that $J - K$ is lower for Sy2s and higher for Sy1s as well as for high luminosity sources. This is interesting considering that at high redshift ($z \approx 1$–2) the reddest EROs are now being used as a means to select obscured type II QSOs (e.g., Brusa et al. 2005).

The authors thank the anonymous referee for useful comments that improved our discussion. We gratefully acknowledge support for this work through the NASA *XMM-Newton* guest observer grant NNX09AP79G. L.M.W. also acknowledges support through the NASA grant HST-HF-51263.01-A, through a Hubble Fellowship from the Space Telescope Science Institute, which is operated by the Association of Universities for Research in Astronomy, Incorporated, under NASA contract NAS5-26555. This work utilizes observations obtained with *XMM-Newton*, an ESA science mission with instruments and contributions directly funded by ESA Member States and NASA. This research has made use of data obtained through the High Energy Astrophysics Science Archive Research Center Online Service, provided by the NASA/Goddard Space Flight Center. Additionally, this research has made use of the NASA/IPAC Extragalactic Database (NED) which is operated by the Jet Propulsion Laboratory, California Institute of Technology, under contract with the National Aeronautics and Space Administration.

REFERENCES

Alexander, D. M., Bauer, F. E., Chapman, S. C., et al. 2005, ApJ, 632, 736
Alexander, D. M., Vignali, C., Bauer, F. E., et al. 2002, AJ, 123, 1149
Antonucci, R. 1993, ARA&A, 31, 473
Arnaud, K. A. 1996, in ASP Conf. Ser. 101, Astronomical Data Analysis Software and Systems V, ed. G. Jacoby & J. Barnes (San Francisco: ASP), 17
Braito, V., Reeves, J. N., Sambruna, R. M., & Gofford, J. 2011, MNRAS, 414, 2739
Brindle, C., Hough, J. H., Bailey, J. A., et al. 1990, MNRAS, 244, 604
Brusa, M., Comastri, A., Daddi, E., et al. 2005, A&A, 432, 69
Crenshaw, D. M., Peterson, B. M., & Wagner, R. M. 1988, AJ, 96, 1208
Dickey, J. M., & Lockman, F. J. 1990, ARA&A, 28, 215
Eckart, M. E., Stern, D., Helfand, D. J., et al. 2006, ApJS, 165, 19
Elitzur, M. 2008, New Astron. Rev., 52, 274
Elston, R., Rieke, G. H., & Rieke, M. J. 1988, ApJ, 331, L77
Garcet, O., Gandhi, P., Gosset, E., et al. 2007, A&A, 474, 473
Hewett, P. C., & Foltz, C. B. 1994, PASP, 106, 113
Koss, M., Mushotzky, R., Veilleux, S., et al. 2011, ApJ, 739, 57
Kraemer, S. B., Crenshaw, D. M., Gabel, J. R., et al. 2006, ApJS, 167, 161
Kraemer, S. B., George, I. M., Crenshaw, D. M., et al. 2005, ApJ, 633, 693
Landi, R., Masetti, N., Morelli, L., et al. 2007, ApJ, 669, 109
Maccacaro, T., Perola, G. C., & Elvis, M. 1982, ApJ, 257, 47
Madrid, J. P., Chiaberge, M., Floyd, D., et al. 2006, ApJS, 164, 307
Magdziarz, P., & Zdziarski, A. A. 1995, MNRAS, 273, 837
Maiolino, R., Marconi, A., & Oliva, E. 2001a, A&A, 365, 37
Maiolino, R., Marconi, A., Salvati, M., et al. 2001b, A&A, 365, 28
Mignoli, M., Pozzetti, L., Comastri, A., et al. 2004, A&A, 418, 827
Morris, S. L., & Ward, M. J. 1989, ApJ, 340, 713
Mushotzky, R. 2004, in Supermassive Black Holes in the Distant Universe, ed. A. J. Barger (Astrophysics and Space Science Library, Vol. 308; Dordrecht: Kluwer), 53
Mushotzky, R. F. 1982, ApJ, 256, 92
Osterbrock, D. E. 1978, Proc. Natl. Acad. Sci., 75, 540
Page, M. J., Carrera, F. J., Stevens, J. A., Ebrero, J., & Blustin, A. J. 2011, MNRAS, 416, 2792
Perola, G. C., Puccetti, S., Fiore, F., et al. 2004, A&A, 421, 491
Risaliti, G., Elvis, M., & Nicastro, F. 2002, ApJ, 571, 234
Severgnini, P., Caccianiga, A., Braito, V., et al. 2006, A&A, 451, 859
Shi, Y., Rieke, G. H., Hines, D. C., et al. 2006, ApJ, 653, 127
Trippe, M. L., Reynolds, C. S., Koss, M., Mushotzky, R. F., & Winter, L. M. 2011, ApJ, 736, 81
Tueller, J., Baumgartner, W. H., Markwardt, C. B., et al. 2010, ApJS, 186, 378
Turner, T. J., Netzer, H., & George, I. M. 1996, ApJ, 463, 134
Ueda, Y., Eguchi, S., Terashima, Y., et al. 2007, ApJ, 664, L79
Ward, M. J., Done, C., Fabian, A. C., Tennant, A. F., & Shafer, R. A. 1988, ApJ, 324, 767
Wilkes, B. J., Pounds, K. A., Schmidt, G. D., et al. 2005, ApJ, 634, 183
Winter, L. M., Lewis, K. T., Koss, M., et al. 2010a, ApJ, 710, 503
Winter, L. M., Mushotzky, R., Lewis, K., et al. 2010b, in AIP Conf. Proc. 1248, X-ray Astronomy 2009: Present Status, Multi-Wavelength Approach and Future Perspectives, ed. A. Comastri, L. Angelini, & M. Cappi (Melville, NY: AIP), 369
Winter, L. M., Mushotzky, R. F., Reynolds, C. S., & Tueller, J. 2009a, ApJ, 690, 1322
Winter, L. M., Mushotzky, R. F., Terashima, Y., & Ueda, Y. 2009b, ApJ, 701, 1644
Winter, L. M., Mushotzky, R. F., Tueller, J., & Markwardt, C. 2008, ApJ, 674, 686